Article No. mb981914 *J. Mol. Biol.* (1998) **281**, 165–181

JMB

Insights into the Mechanism of Heterodimerization from the ^{1}H-NMR Solution Structure of the c-Myc-Max Heterodimeric Leucine Zipper

Pierre Lavigne, Matthew P. Crump, Stéphane M. Gagné Robert S. Hodges, Cyril M. Kay* and Brian D. Sykes*

The Protein Engineering Network of Centres of Excellence, Department of Biochemistry, University of Alberta, Edmonton, Alberta Canada T6G 2S2

**Corresponding authors*

The oncoprotein c-Myc (a member of the helix-loop-helix-leucine zipper (b-HLH-LZ) family of transcription factors) must heterodimerize with the b-HLH-LZ Max protein to bind DNA and activate transcription. It has been shown that the LZ domains of the c-Myc and Max proteins specifically form a heterodimeric LZ at 20°C and neutral pH. This suggests that the LZ domains of the c-Myc and Max proteins are playing an important role in the heterodimerization of the corresponding gene products *in vivo*. Initially, to gain an insight into the energetics of heterodimerization, we studied the stability of N-terminal disulfide-linked versions of the c-Myc and Max homodimeric LZs and c-Myc-Max heterodimeric LZ by fitting the temperature-induced denaturation curves monitored by circular dichroism spectroscopy. The c-Myc LZ does not homodimerize (as previously reported) and the c-Myc-Max heterodimeric LZ is more stable than the Max homodimeric LZ at 20°C and pH 7.0. In order to determine the critical interhelical interactions responsible for the molecular recognition between the c-Myc and Max LZs, the solution structure of the disulfide-linked c-Myc-Max heterodimeric LZ was solved by two-dimensional ^{1}H-NMR techniques at 25°C and pH 4.7. Both LZs are α-helical and the tertiary structure depicts the typical left-handed superhelical twist of a two-stranded parallel α-helical coiled-coil. A buried salt bridge involving a histidine on the Max LZ and two glutamate residues on the c-Myc LZ is observed at the interface of the heterodimeric LZ. A buried H-bond between an asparagine side-chain and a backbone carbonyl is also observed. Moreover, evidence for *e-g* interhelical salt bridges is reported. These specific interactions give insights into the preferential heterodimerization process of the two LZs. The low stabilities of the Max homodimeric LZ and the c-Myc-Max heterodimeric LZ as well as the specific interactions observed are discussed with regard to regulation of transcription in this family of transcription factors.

Keywords: leucine zippers; two-dimensional ^{1}H-NMR; solution structure; H-bonds; buried salt bridge

Introduction

The proteins from the proto-oncogene *myc* family (c-Myc, N-Myc and L-Myc) are thought to govern important cellular processes such as cell cycle entry, proliferation and differentiation (Henriksson & Lüscher, 1996, and references therein). To bind to DNA, activate transcription and perform its oncongenic activity, c-Myc has to heterodimerize with the protein Max (Blackwood & Eisenman, 1991; Amati *et al*., 1992, 1993; Kretzner *et al*., 1992). Max is also known to heterodimerize

Abbreviations used: b-HLH-LZ, basic region-helix-loop-helix-leucine zipper; CD, circular dichroism; DQF-COSY, double quantum filtered two-dimensional correlated spectroscopy; NMR, nuclear magnetic resonance spectroscopy; NOE, nuclear Overhauser effect; NOESY, nuclear Overhauser enhancement spectroscopy; r.m.s.d., root-mean-square deviation; TOCSY, total correlation spectroscopy; ppm, parts per million.

E-mail address of the corresponding author: bds@polaris.biochem.ualberta.ca

0022–2836/98/310165–17 $30.00/0

with proteins from the *mad* family (Mad, Ayer *et al.*, 1993; Mad3, Mad4, Hurlin *et al.*, 1995; and Mxi1, Zervos *et al.*, 1993) as well as the newly discovered protein Mnt (Hurlin *et al.*, 1997). Mad-Max, Mad3-Max, Mad4-Max, Mxi1-Max and Mnt-Max heterodimers behave as c-Myc antagonists. All the Max heterodimers and the Max homodimer have been shown to bind the same DNA sequence (Henriksson & Lüscher, 1996; Hurlin *et al.*, 1997). The Max protein is long lived and expressed at a nearly constant level so that the cellular activities of the proteins of the short lived Myc and Mad families are thought to be controlled by the level and the temporal pattern of expression of their corresponding genes (Henriksson & Lüscher, 1996). The association of Max with its partners is thought to occur through the heterodimerization of their HLH-LZ domains. The crystal structure of the Max homodimer bound to its cognate DNA sequence revealed that the HLH domains fold into a parallel four-helix bundle and that LZ domains fold as a parallel two-stranded α-helical coiled-coil (Ferré-D'Amaré *et al.*, 1993). Although Max can homodimerize and bind DNA, none of its partners can. This underscores the importance for efficient molecular recognition of the Max partners through the heterodimerization of HLH-LZ domains. In this context, it is important to investigate the putative role of the LZ domains of this sub-family of transcription factors in the molecular recognition of Max and its partners.

In two previous studies, it was shown that the c-Myc and Max LZs preferentially form a heterodimer (Lavigne *et al.*, 1995; Muhle-Goll *et al.*, 1995). This has led to the proposal that the LZ domains of Max and c-Myc are responsible for the specificity or molecular recognition *in vivo*. In the same two studies, molecular models describing interhelical salt bridges and hydrogen bonds that might be responsible for the specificity were described. A salt bridge between an unusual histidine at a position *d* on the Max LZ and two glutamate residues at positions *a* on the c-Myc LZ was proposed to be critical for molecular recognition (Lavigne *et al.*, 1995). The existence of the salt bridge in that model was supported by the fact that the pK_a value of the histidine in the folded form of the c-Myc-Max heterodimeric LZ was elevated compared to the pK_a value in the unfolded form (Lavigne *et al.*, 1995). Interestingly, an acidic residue is conserved in the LZ domains of all the Max interacting proteins known to date in the corresponding position of one of the glutamate residues proposed to interact with the histidine on the Max LZ.

Here we describe the solution structure of the c-Myc-Max heterodimeric LZ and the relative stabilities of the N-terminal disulfide-linked c-Myc and Max homodimeric LZs and c-Myc-Max heterodimeric LZ. As for other dimeric LZs, the c-Myc-Max heterodimeric LZ is a two-stranded and parallel α-helical coiled-coil. The solution structure reveals the existence of the proposed salt bridge between the histidine on the Max LZ and the two glutamate residues on the c-Myc LZ. Other specific interhelical interactions are also reported. Based on the structural data presented, we propose that the buried salt bridge might be conserved throughout the different Max heterodimers and that the LZ domains therefore play a crucial role in the regulation of this family of b-HLH-LZ transcription factors.

Results and Discussion

Energetics of the preferential heterodimerization of the c-Myc and Max LZs

Figure 1A represents the amino acid sequence of the c-Myc LZ (Battey *et al.*, 1983) and the Max LZ (Prendergast *et al.*, 1991) according to the heptad repeat: *a-b-c-d-e-f-g* typical for coiled-coil forming proteins (Hodges *et al.*, 1972; Stone *et al.*, 1975; Cohen & Parry, 1990; Hodges, 1992, 1996). A helical wheel diagram schematically describing putative interhelical electrostatic interactions is displayed in Figure 1B.

In order to gain more insights into the mechanism of heterodimerization, the stability of the disulfide-linked c-Myc and Max LZs and the c-Myc-Max LZ was studied by temperature-induced denaturation monitored by CD spectroscopy at pH 7.0. The typical α-helical far-ultraviolet CD spectra of the three disulfide-linked LZs were described elsewhere (Lavigne *et al.*, 1995). Figure 2A illustrates the temperature-induced denaturation curves for the disulfide-linked c-Myc and Max LZs and the c-Myc-Max heterodimeric LZ. The temperature denaturation curve of the disulfide-linked c-Myc LZ does not depict any coop-

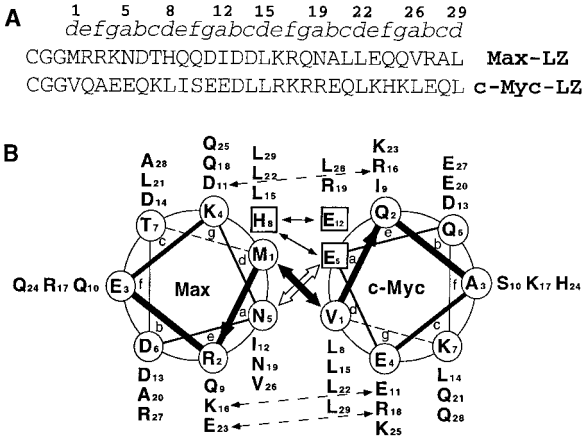

Figure 1. A, Primary structures of the c-Myc (Battey *et al.*, 1983) and Max (Prendergast *et al.*, 1991) LZs displayed with the classical *a-b-c-d-e-f-g* heptad repeat pattern. B, Helical wheel diagram of the c-Myc-Max heterodimeric LZ. Thin arrows describe putative interhelical electrostatic interactions described elsewhere (Lavigne *et al.*, 1995; Muhle-Goll *et al.*, 1995). Synthetic peptides were N-acetylated and C-amidated. The homodimeric and heterodimeric LZs were disulfide-linked by air oxidation of the cysteine side-chains.

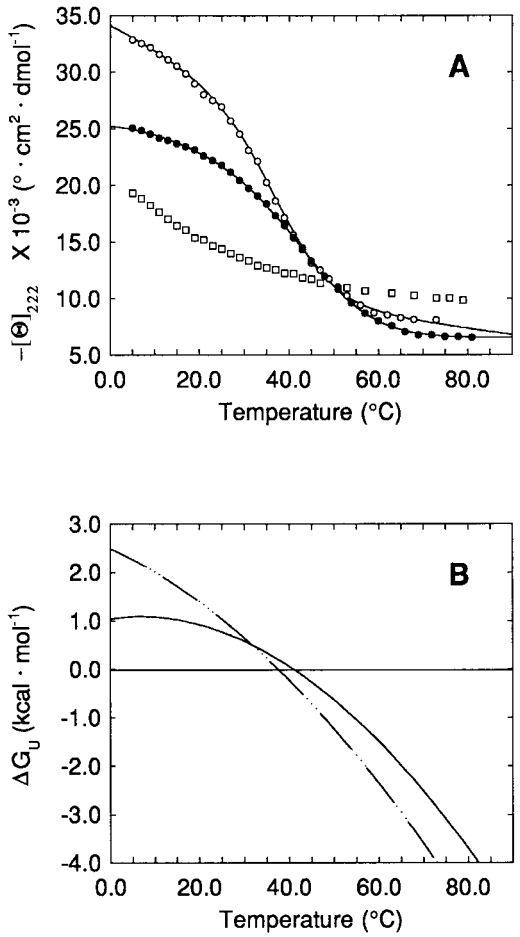

Figure 2. Temperature-induced denaturations monitored by the change in mean residue ellipticity at 222 nm ($-\Theta_{222}$). A, Temperature-induced denaturation of the disulfide-linked c-Myc homodimeric LZ (open squares), Max homodimeric LZ (filled circles) and the c-Myc-Max heterodimeric LZ (open circles) recorded in 50 mM potassium phosphate, 50 mM KCl (pH 7.0). B, The corresponding stability curves obtained from the non-linear least-squares fitting as described in Materials and Methods. The parameters obtained for the Max homodimeric LZ (continuous line) are the following: $T^{o} = 41.0°C$, $\Delta H^{o}_{u} = 19.6$ kcal·mol^{-1}, $\Delta C_{p,u} = 0.54$ kcal·mol^{-1}·K^{-1}, $\Theta_N(0) = 28{,}000$, $d\Theta_N(T)/dT = 0.10$, $\Theta_U(0) = 6{,}200$, $d\Theta_U(T)/dT = -0.004$ and those obtained for the c-Myc-Max heterodimeric LZ (dotted line) are: $T^{o} = 38°C$, $\Delta H^{o}_{u} = 28.3$ kcal·mol^{-1}, $\Delta C_{p,u} = 0.39$ kcal·mol^{-1}·K^{-1}, $\Theta_N(0) = 34{,}400$, $d\Theta_N(T)/dT = 0.19$, $\Theta_U(0) = 12{,}100$, $d\Theta_U(T)/dT = 0.06$. The denaturation curve of the c-Myc homodimeric LZ was not fitted due to the absence of an apparent cooperative transition.

erative transition in accordance with previous studies that have shown that the c-Myc LZ does not homodimerize (Muhle-Goll *et al.*, 1994; Lavigne *et al.*, 1995). The denaturation curves of the disulfide-linked Max homodimeric and c-Myc-Max heterodimeric LZs have been fitted assuming a two-state transition as described in Materials and Methods. A heat capacity of unfolding ($\Delta C_{p,u}$) of 0.39 kcal·mol^{-1}·K^{-1} was used for the fitting of the disulfide-linked c-Myc-Max heterodimeric LZ temperature denaturation curve. The $\Delta C_{p,u}$ was obtained from the linear relationship between the van't Hoff enthalpy and the melting temperature obtained from temperature-induced denaturations carried out at different pH values (Privalov, 1979) and is in good agreement with the one reported for the GCN4 homodimeric LZ (Kenar *et al.*, 1995). For the fitting of the temperature-induced denaturation of the disulfide-linked Max homodimeric LZ, a $\Delta C_{p,u}$ of 0.55 kcal·mol^{-1}·K^{-1} was used in order to obtain the best possible fit.

The mean residue ellipticities at 222 nm recorded for the disulfide-linked Max homodimeric LZ at low temperature (<30°C) are lower than those of the disulfide-linked c-Myc-Max heterodimeric LZ. At 5°C the mean residue ellipticity of the disulfide-linked Max homodimeric LZ is 25,100 deg.·cm^2·dmol^{-1}, corresponding to approximately 75% of the predicted mean residue ellipticity for a fully helical peptide of that length (33,350 deg.·cm^2·dmol^{-1}; Chen *et al.*, 1974). On the other hand, the mean residue ellipticity at 222 nm of the disulfide-linked c-Myc-Max heterodimeric LZ (32,100 deg.·cm^2·dmol^{-1}) is close to the theoretical value for a fully helical peptide of that length. Therefore, assuming a two-state unfolding reaction, it is to be expected that the population of folded disulfide-linked Max homodimeric LZ will be lower than that of the c-Myc-Max heterodimeric LZ at temperatures below 30°C.

The corresponding stability curves ($\Delta G_u(T)$) for the disulfide-linked Max homodimeric LZ and c-Myc-Max heterodimeric LZ are shown in Figure 2B. It is noted that the c-Myc-Max heterodimeric LZ is more stable than the Max homodimeric LZ at temperatures below 30°C. Interestingly, the ΔG_u value at 5°C for the disulfide-linked Max homodimeric LZ obtained from the fitting is 1.1 kcal·mol^{-1}, which corresponds to a population of the unfolded state of 0.12, a figure in near agreement with the mean residue ellipticity observed. With a ΔG_u value at 5°C of 2.3 kcal·mol^{-1}, a population of the unfolded state of 0.02 can be estimated for the disulfide-linked c-Myc-Max heterodimeric LZ again in accordance with the mean residue ellipticity observed. The higher stability of the c-Myc-Max heterodimeric LZ compared to that of the Max homodimeric LZ at temperatures lower than 30°C, coupled to the fact that the c-Myc LZ does not homodimerize rationalizes the preferential heterodimerization previously observed at 20°C and pH 7.0 (Lavigne *et al.*, 1995). On the other hand, it should be noted that the disulfide-linked Max homodimeric LZ and c-Myc-Max heterodimeric LZ have a low melting temperature of approximately 37°C. It is to be expected that the heterodimerization will be less specific at 37°C compared to room temperature. Nonetheless, even if the Max homodimeric LZ and the c-Myc-Max heterodimeric LZ have low stabilities, taking into account that the c-Myc LZ does not homodimerize, the folded c-Myc-Max heterodi-

meric LZ will always be preferred over the folded Max homodimeric LZ in a concentration-dependent way (mass action or Le Châtelier Principle; Atkins, 1982).

The ^{1}H-NMR solution structure of the N-terminal disulfide-linked c-Myc-Max heterodimeric LZ

In a previous study, we have shown that the melting temperature of the disulfide-linked c-Myc-Max heterodimeric LZ was increased by 10 deg.C when the pH was decreased from 7.0 to 5.0 (Lavigne *et al.*, 1995). In Figure 3A, we present the fitted temperature-induced denaturation curve obtained at pH 5.0 and in Figure 3B the corresponding stability curve compared to the one obtained at pH 7.0 (see Figure 2B). One can see that the stability curve obtained at pH 5.0 is shifted up by about 1 kcal·mol^{-1}. The increase in stability was ascribed to the presence of a salt bridge involving Max His8*d* and the c-Myc Glu5*a* and Glu12*a* (Lavigne *et al.*, 1995). Consequently all the NMR spectra were acquired at pH 4.8 and 25°C. Under these conditions the stability of the disulfide-linked c-Myc-Max heterodimeric LZ is approximately 2.1 kcal·mol^{-1}, which corresponds to a population for the folded form that is greater than 0.97. Although the stability of the disulfide-linked c-Myc-Max heterodimeric LZ is found to increase below 25°C (Figures 2B, 3B), the conditions were the best compromise between narrow linewidths and amount of folded peptide.

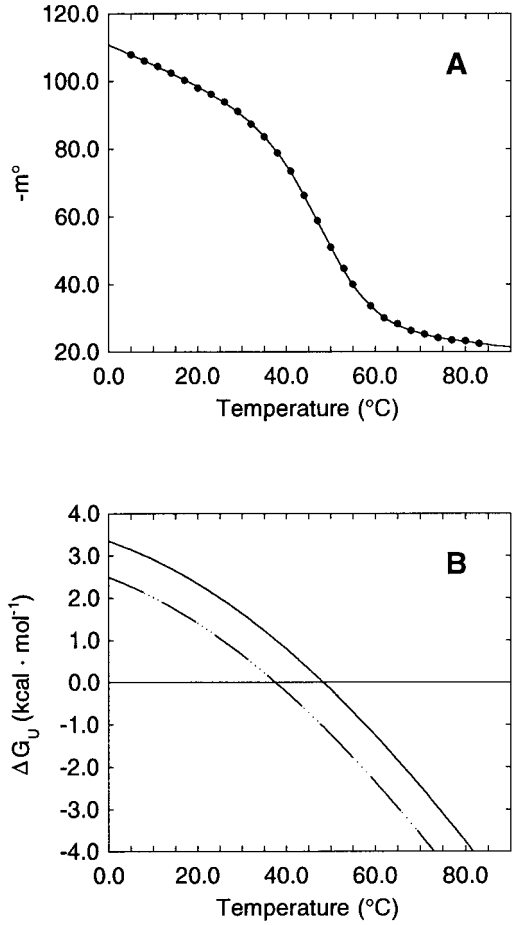

Figure 3. A, Temperature-induced denaturation of the disulfide-linked c-Myc-Max heterodimeric LZ recorded by monitoring the ellipticity readings at 222 nm (in m°) in 50 mM potassium phosphate, 50 mM KCl (pH 5.0). B, The corresponding stability curves (continuous line) obtained from the non-linear least-squares fitting as described in Materials and Methods. Also shown in B for the sake of comparison is the stability curve of the disulfide-linked c-Myc-Max LZ at pH 7.0 (discontinuous line and as shown in Figure 2B). The fitted parameters obtained for the c-Myc-Max heterodimeric LZ at pH 5.0 (continuous line) are: $T^\circ = 48.4$°C, $\Delta H^\circ_u = 32.3$ kcal·mol^{-1}, $\Delta C_{p,u} = 0.39$ kcal·mol^{-1}·K^{-1}, $m^\circ_N(0) = 111.0$, $dm^\circ_N(T)/dT = 0.58$, $m^\circ_U(0) = 34.5$, $dm^\circ_U(T)/dT = 0.14$. Note that the stability curve at pH 5.0 is shifted up by almost 1 kcal·mol^{-1} in comparison to pH 7.0.

NMR restraints

As expected for two-dimensional ^{1}H-NMR of α-helical proteins without aromatic residues (phenylalanine, tryptophan and tyrosine), spectral analysis was complicated by strong overlap in the fingerprint region of DQF-COSY, NOESY and TOCSY spectra and also by poor coherence transfer on TOCSY spectra. Despite the overall poor dispersion of H^α chemical shifts, well resolved α-helical like H^α resonances belonging to residues such as valine, isoleucine, aspartate, asparagine and histidine were observed. Coupled to a good dispersion of the backbone NH resonances (7.2 to 9.0 ppm), the well resolved H^α chemical shifts enabled the assignment of a significant number of sequential (e.g. strong d_{NN} and weak $d_{\alpha N}$) and medium range (e.g. $d_{\alpha N}$ $(i, i+3)$ and $(i, i+4)$) α-helical connectivities dispersed throughout the c-Myc and the Max LZs. Well resolved interfacial side-chain ^{1}H resonances allowed for the assignment of 60 long range interhelical connectivities.

A total of 430 NOE-derived distance restraints consisting of 115 sequential, 119 medium range, 136 intraresidue and 60 long range NOE contacts were used for the structure calculations. The distribution of the NOEs per residue is shown in Figure 4A and B. 15 χ1, 50 ϕ angles and 50 restraints for 50 backbone hydrogen bonds (CO–N = 2.4 to 3.3 Å) were also included for the calculation of the structures (see Materials and Methods).

Quality of the calculated structures

A family of 40 structures collectively called ⟨c-Myc-Max⟩ was calculated using the program X-PLOR (Brünger, 1992). The structural statistics of ⟨c-Myc-Max⟩ are presented in Table 1. The quality of the 40 structures is very high as judged by small deviations from idealized covalent geometry and good fit to the experimental NMR data. The local

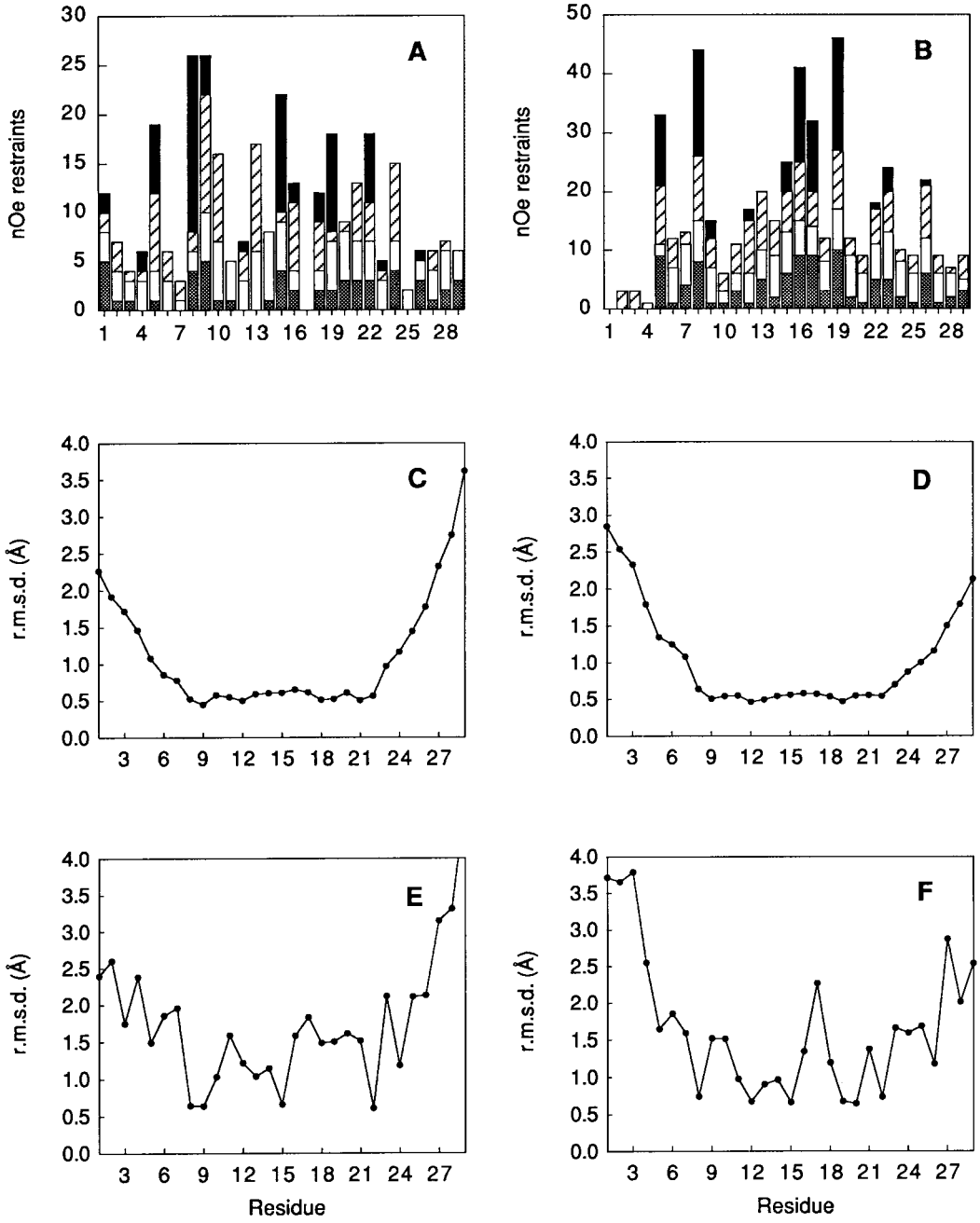

Figure 4. Structural data for ⟨c-Myc-Max⟩ plotted as a function of the residue number for the c-Myc and Max LZ. A and B, Distribution of NOE restraints for the c-Myc and Max LZ, respectively. Grey, white, hatched and black bars represent intraresidue, sequential, medium range and long range restraints, respectively. C and D, the mean r.m.s.d. as a function of the residue number for the backbone (C^{α}, C′, O, N) atoms of the c-Myc and Max LZ, respectively. E and F, the mean r.m.s.d. as a function of the residue number for the heavy atoms of the c-Myc and Max LZ, respectively. The r.m.s.d. values are obtained from the fitting of backbone atoms of residues 5 to 25 of ⟨c-Myc-Max⟩ onto $\overline{\text{c-Myc-Max}}$.

angle geometry of the 40 structures was analyzed with PROCHECK (Laskowski *et al.*, 1993) for the three main angles ϕ, ψ, χ^1; 99% of the (ϕ,ψ) angles lie in the most favored and additionally allowed regions of the Ramachandran plot. An average structure denoted $\overline{\text{c-Myc-Max}}$ was calculated from the coordinates of ⟨c-Myc-Max⟩. Figure 5 represents a best fit superimposition of the backbone of ⟨c-Myc-Max⟩ with the backbone of the $\overline{\text{c-Myc-Max}}$. In Figure 4C and D, we present the mean r.m.s.d. by residue for the backbone atoms of ⟨c-Myc-Max⟩ *versus* $\overline{\text{c-Myc-Max}}$ for the c-Myc and Max LZs, respectively. Collectively, the mean r.m.s.d. for residues 5 to 25 of both LZs amounts to 0.66(±0.23) Å. It is evident from Figure 4C and D that a better definition of the backbone of each LZ has been achieved towards the center of the heterodimer where a larger number of distance restraints

Table 1. Structural statistics and atomic r.m.s.d. for the c-Myc-Max LZ

	⟨c-Myc-Max⟩	$\overline{\text{c-Myc-Max}}$ r
r.m.s.d. from experimental restraints (Å)[a] All (480)		
Interresidue (centered averaged)		
Long ($\|i-j\|>5$)	0.0015 ± 0.0023	0.000
Medium ($1 \leqslant \|i-j\| \leqslant 5$)	0.0182 ± 0.0015	0.018
Sequential ($\|i-j\|=1$)	0.0031 ± 0.0015	0.004
H-bonds	0.0023 ± 0.0019	0.001
Intraresidue (center averaged)	0.0059 ± 0.0040	0.002
Dihedral angles	0.0076 ± 0.0021	0.000
E_{NOE} (kcal·mol^{-1})[b]	2.436 ± 0.639	2.14
E_{DIH} (kcal·mol^{-1})[b]	0.0019 ± 0.0067	0
E_{REPEL} (kcal·mol^{-1})[b]	13.13 ± 1.19	11.70
Deviations from idealized geometry[c]		
Bonds (Å)	0.0016 ± 0.0001	0.0015
Angles (deg.)	0.3546 ± 0.0070	0.345
Impropers (deg.)	0.1690 ± 0.0053	0
r.m.s.d. (Å)		
Backbone atoms[d]	1.09 ± 0.58	
Heavy atoms[d]	1.73 ± 0.80	
Best defined region		
Backbone atoms[e]	0.66 ± 0.23	
Heavy atoms[e]	1.29 ± 0.48	

[a] The r.m.s.d. values of the experimental restraints were calculated with respect to the upper and lower limits of the input restraints.
[b] The values for E_{NOE} and E_{DIH} are calculated from a square well potential with a force constant of 50 kcal·mol^{-1}·Å^{-2} and 200 kcal·mol^{-1}·rad^{-2}. E_{REPEL} is calculated with a force constant of 4 kcal·mol^{-1}·Å^{-4} and the final van der Waals radii were set to 0.8 times the values used in the CHARMM force field.
[c] The values for bonds, angles and impropers show the deviation from ideal values based on perfect stereochemistry.
[d] Combined average of both the c-Myc and Max LZs for residues 1 to 29 (excluding the Cys-Gly-Gly linkers).
[e] Combined average of both the c-Myc and Max LZs for residues 5 to 25 (best defined region).

could be observed. The observation of more disordered N and C termini agrees with the comparatively fewer restraints observed in the first and last heptads. Figure 4E and F displays the mean r.m.s.d. per residue for all the heavy atoms of ⟨c-Myc-Max⟩ *versus* $\overline{\text{c-Myc-Max}}$ for the c-Myc and Max LZs, respectively. The overall r.m.s.d. value for residues 5 to 25 of each LZ is 1.29(±0.48) Å. Minima with a mean r.m.s.d. value close to 0.5 Å are observed for most residues occurring at the interfacial positions *a* and *d*, indicating that they are well defined by the restraints.

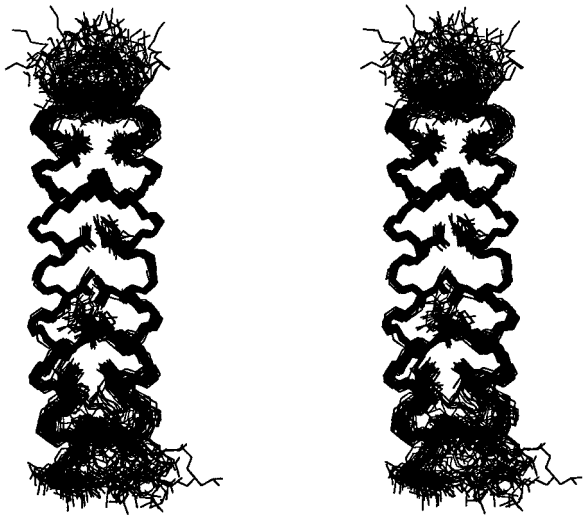

Figure 5. Stereo view of the best-fit superposition of the backbone atoms of residues 5 to 25 of ⟨c-Myc-Max⟩ onto the corresponding atoms of $\overline{\text{c-Myc-Max}}$. The C^{α}, C and N backbone atoms and the heavy atoms of interfacial side-chains (positions *a* and *d*) are shown. The c-Myc LZ is the helix on the right and the Max LZ is the helix on the left of the heterodimer structure with the N termini at the top and the C termini at the bottom. The Figure was generated using the program Insight II (Biosym, Palo Alto, CA).

$\overline{\text{c-Myc-Max}}$ was regularized with restrained minimization (2000 steps) in order to fix poor covalent geometry and non-covalent contacts to yield the final structure $\overline{\text{c-Myc-Max}}$ r. The final minimized structure shows no NOE violations >0.2 Å, no dihedral angle violations > 0.3°, and possesses good covalent geometry and non-bonded contacts as evidenced by small values for the van der Waals energy (E_{REPEL}). A single Ramachandran analysis generated for $\overline{\text{c-Myc-Max}}$ r shows that greater than 98% of residues are in the most favored core region.

Tertiary structure

Ribbon diagrams of $\overline{\text{c-Myc-Max}}$ r with the interfacial side-chains (positions *a* and *d*) displayed are presented in Figure 6A and B. One can clearly see that the two LZs fold as curved helices that wrap around each other. One also observes from Figure 6C the typical left-handed superhelical twist observed in parallel and two-stranded α-helical coiled-coils. When the backbone of residues 1 to 29

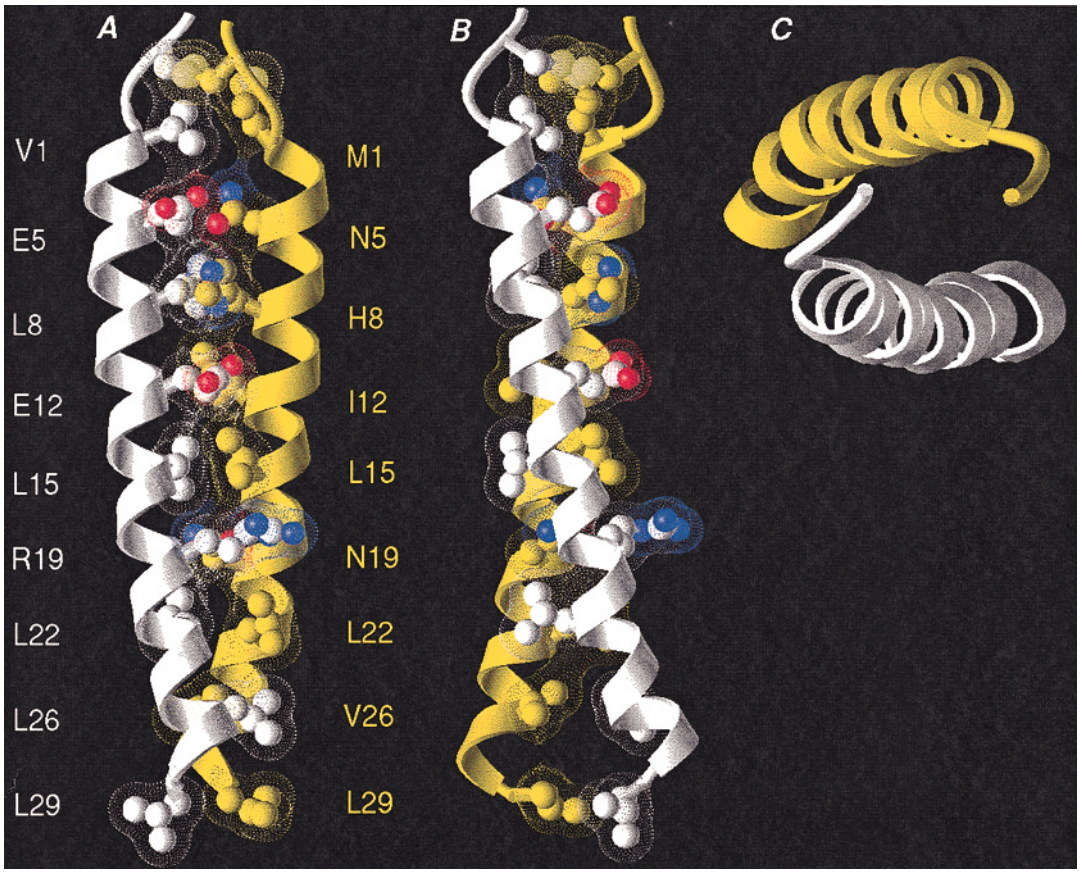

Figure 6. Ribbon diagrams of the minimized average structure (c-Myc-Max r) schematically depicting its tertiary structure. A and B, Side-views of c-Myc-Max r with the backbone atoms represented by the ribbons onto which the interfacial side-chains and their corresponding molecular surfaces (positions *a* and *d*) are attached. The yellow ribbon and carbon atoms belong to the Max LZ and the white ribbon and carbon atoms belong to the c-Myc LZ. C, Top view without the side-chains. Note the curvature of both helices and the left-handed super-helical twist. The Figure was prepared with the program Ribbons (Carson, 1987).

of each LZ of c-Myc-Max r is superimposed on the backbone atoms of corresponding residues of the GCN4 homodimeric LZ crystal structure (O'Shea *et al.*, 1991), a r.m.s.d. value of 0.74 Å is obtained, indicating a close similarity between the backbone of the two structures (not shown). The helix curvature in two-stranded α-helical coiled-coils has been shown to be correlated with a periodicity of CO–HN (i, $i+4$) H-bond lengths, i.e. the H-bonds involving the amide protons of the interfacial positions *a*, *d* and *e* were found to be shorter than the ones for the exposed positions *b*, *c*, *f* and *g* (O'Shea *et al.*, 1991). Interestingly, the same periodicity was observed for predicted H-bond lengths (Pardi *et al.*, 1983) calculated from the amide protons chemical shift assignments for the GCN4 LZ (Kuntz *et al.*, 1991; Goodman & Kim, 1991). This periodicity was also observed for the c-Jun LZ (Junius *et al.*, 1993). Using the empirical equation described by Pardi *et al.* (1983), the random coil values for amide protons (Wishart *et al.*, 1995) and the average amide protons chemical shift at the different heptad position for the c-Myc-Max heterodimeric LZ, we calculated the predicted average H-bond lengths for the different heptad positions for both LZs. For the Max LZ, the predicted positional CO–HN (i, $i+4$) H-bond lengths are: *a* (1.93(±0.07) Å), *b* (2.07(±0.07) Å), *c* (2.14(±0.10) Å), *d* (2.05(±0.11) Å), *e* (1.93(±0.02) Å), *f* (2.17(±0.08) Å) and *g* (2.07(±0.09) Å) and for the c-Myc LZ are: *a* (1.99(±0.04) Å), *b* (2.13(±0.13) Å), *c* (2.10(±0.12) Å), *d* (2.00(±0.09) Å), *e* (1.95(±0.02) Å), *f* (2.08(±0.06) Å) and *g* (2.11(±0.06) Å). Again, the same tendency for predicted buried H-bonds to be shorter than the exposed ones is observed. Upon inspection of the CO–HN (i, $i+4$) H-bond lengths of the final structure, we also observe a tendency for the buried CO–HN (i, $i+4$) H-bonds (positions *a*, *d* and *e*) to be shorter. It should be noted that the curvature of the helices (and the distribution of CO–HN (i, $i+4$) H-bond lengths) is solely driven by long range and interhelical NOEs, since all the CO–N (i, $i+4$) used in the calculation were conservative, had the same upper (3.3 Å) and lower bound (2.4 Å) and were not forced to linearity.

Packing of the leucine residues at position d

The dihedral angles (χ1 and χ2) of the conserved and well defined leucine side-chains at positions *d* (i.e. all the leucine residues found at position *d* except c-Myc Leu 29*d* and Max Leu 29*d*) have

average values of $\chi1 = -79(\pm9)^\circ$ and $\chi2 = 159(\pm12)^\circ$. These values are in excellent agreement with previously reported values for the crystal structure of the GCN4 homodimeric LZ ($\chi1 = -69^\circ$ and $\chi2 = 155^\circ$; O'Shea *et al.*, 1991) and the NMR structure of the c-Jun homodimeric LZ ($\chi1 = -86^\circ$ and $\chi2 = 156^\circ$; Junius *et al.*, 1996). We show in Figure 7A the packing of the pair of leucine side-chains at positions 15*d*. Complementariness of side-chain packing that includes the participation of the side-chains at positions *e* is seen, in agreement with the knobs-into-holes model (Crick, 1953; O'Shea *et al.*, 1991). Moreover, all the leucine side-chains at positions *d* pack in the perpendicular fashion as defined by the angle between the C^α–C^β bonds and the peptide bond linking residues at positions *d* and *e* (O'Shea *et al.*, 1991; Harbury *et al.*, 1993).

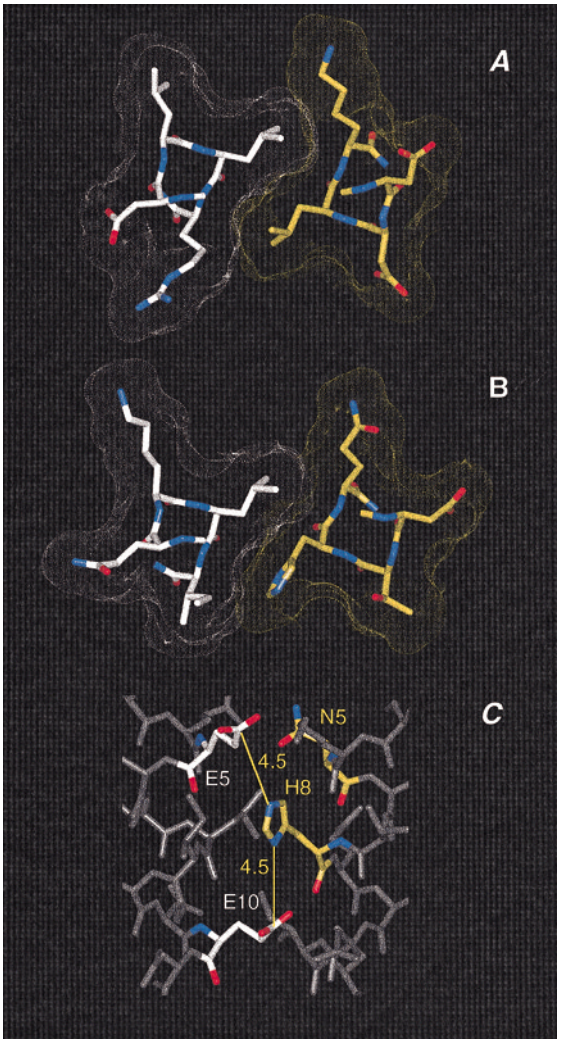

Figure 7. A, Cross-sectional view of c-Myc-Max r depicting the interfacial arrangement of c-Myc Leu15*d* and Max Leu15*d* and the complementariness of the corresponding molecular surfaces. Note the perpendicular packing of the leucine side-chains as defined by the relative orientation of the C^α–C^β bonds and the peptide bond linking residues at positions *d* and *e* on the opposing helix (Harbury *et al.*, 1993). B, Interfacial arrangement of c-Myc Leu8*d* and Max His8*d* and the complementariness of the corresponding molecular surfaces. Again note the perpendicular packing of the leucine and histidine side-chains. C, Interhelical interactions between Max His8*d* and c-Myc Glu5*a* and c-Myc Glu12*a*. Same color code as for Figure 6. See the text for further details. Distances are given in Å. The Figure was generated using the program Insight II (Biosym, Palo Alto, CA).

Packing of the histidine at position d

It has been proposed that the histidine at position 8*d* on the Max LZ plays a key role in its preferential heterodimerization with the c-Myc LZ (Lavigne *et al.*, 1995). The structure reveals that the histidine side-chain is 85% buried, and Figure 7B shows the molecular surface complementariness of this side-chain at the interface of the heterodimeric LZ. The conformation of the side-chain of Max His8*d* is well defined with more than 40 NOE-derived distance restraints resulting in a mean r.m.s.d. value of 0.68 Å for all the heavy atoms of that residue and $\chi1$ and $\chi2$ values of $-81(\pm8)^\circ$ and $-57(\pm7.0)^\circ$, respectively. In this conformation the $H^{\delta2}$ of Max His8*d* points up in the direction of Max

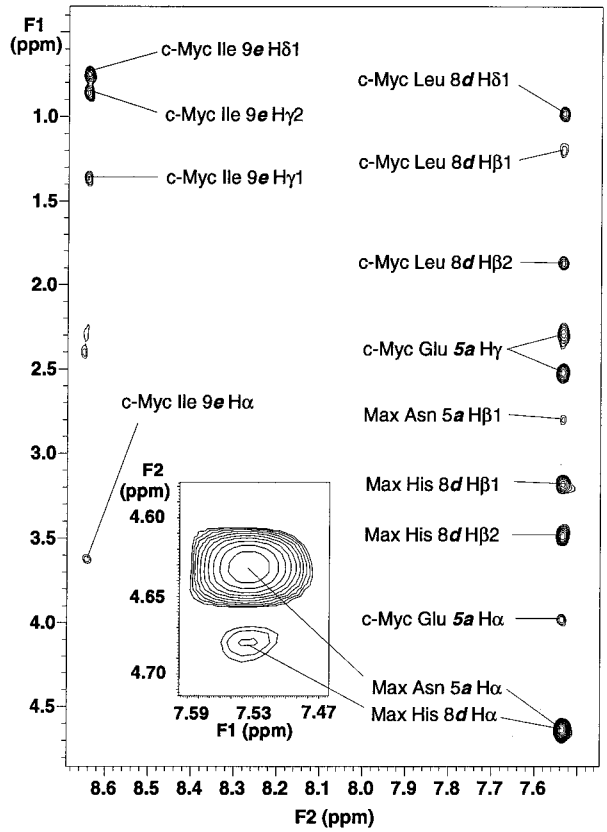

Figure 8. Section of a 500 MHz NOESY spectrum (mixing time 150 ms) recorded in 100% ^2H_2O and after exchange of all exchangeable amide protons. Labeled are intraresidue, sequential and long range NOEs between the $H^{\delta2}$ (7.53 ppm) and the $H^{\varepsilon1}$ (8.65 ppm) of Max His8*d*. Inset: transposed dimension showing the resolved intraresidue and medium range NOEs between the $H^{\delta2}$ of Max His8*d* and its own H^α and the H^α of Max Asn5*a*.

Asn5*a* and away from its own H^{α}. As shown in the inset of Figure 8, a strong medium range NOE between the $H^{\delta 2}$ of Max His8*d* and the H^{α} of Asn5*a* is observed as well as a weak intraresidual NOE between its own $H^{\delta 2}$ and H^{α}. Max His8*d* packs between c-Myc Leu8*d* and c-Myc Ile9*e* (Figure 7B) and long range NOEs between Max His8*d* $H^{\delta 2}$ and $H^{\varepsilon 1}$ to the side-chains of these residues (Figure 8) further confirms the orientation of the histidine side-chain. The histidine $C^{\delta 2}$ is within van der Waals contact of the $C^{\delta 1}$ and C^{β} on the opposing c-Myc Leu8*d* and the C^{α} of Max Asn5*a*, while the two imidazole nitrogen atoms are pointing away from the interface. As seen in Figure 7C the $N^{\delta 1}$ is directed up towards c-Myc Glu5*a* and the $N^{\varepsilon 2}$ is directed towards c-Myc Glu12*a* leading to the formation of a salt bridge and/or charged H-bonds. It has to be noted that the side-chains of c-Myc Glu5*a* and c-Myc Glu12*a* are 75% and 85% buried, respectively. Hence the burial of Max His8*d* appears to depend critically on the amphipathic nature of its side-chain as it participates in both hydrophobic and polar interactions at the interface of the c-Myc-Max heterodimeric LZ.

Packing of the asparagine residues at position a

The occurrence of asparagine residues at positions *a* of the heptad repeat of coiled-coil forming proteins is a conserved feature (Hu & Sauer, 1992; Hurst, 1994; Blake *et al*., 1995). It has been demonstrated that the asparagine residues are promoting formation of homodimeric LZs (Harbury *et al*., 1993; Junius *et al*., 1995; Lumb & Kim, 1995a; Gonzalez *et al*., 1996) most likely by destabilizing higher-order oligomers (trimeric and/or tetrameric). This conferred dimer specificity is effected at the expense of stability (Harbury *et al*., 1993; Junius *et al*., 1995; Lumb & Kim, 1995a) but on the other hand the reduced stability facilitates reassortment of LZs (Wendt *et al*., 1995). Although many studies have focused on the role and the interactions of the conserved asparagine in homodimeric LZs, less attention has been paid to their packing in heterodimeric LZs.

Figure 9A and B illustrates the packing of Max Asn5*a* and Asn19*a*. Both side-chains are buried, although the complementariness of the molecular surfaces surrounding Max Asn19*a* appears more ideal. The apparent less complementary packing of Max Asn5*a* might reflect local unfolding in the folded state as manifested by the lower number of NOEs and concomitant lower definition of this region of the structure. This agrees with the faster ^{1}H to ^{2}H exchange rate observed for the side-chain of Max Asn5*a* that may be more readily solvent accessible if local unfolding occurs in the folded state of the disulfide-linked c-Myc-Max heterodimeric LZ (Lavigne *et al*., 1997). In the crystal structure of the c-Fos-c-Jun heterodimer, the conserved asparagine at a position *a* on the c-Jun LZ forms charged H-bonds with the glutamate side-chain at the flanking position *g* on the c-Fos LZ (Glover & Harrison, 1995). Interestingly, a similar interaction could occur in the c-Myc-Max heterodimeric LZ between Max Asn5*a* and c-Myc Glu4 *g* (Figure 9C). Unfortunately, the overall definition in the first five residues of the structure is not sufficient to conclude if such an interaction exists. In our previous model, we proposed that the $N^{\delta 2}$ of Asn5*a* was pointing towards c-Myc Glu5*a* in order to alleviate, through H-bonding (internal solvation), some of the loss of solvation free energy that would ensue the burial of the carboxylate of c-Myc Glu5*a*. Ongoing studies on a longer version of the c-Myc-Max heterodimeric

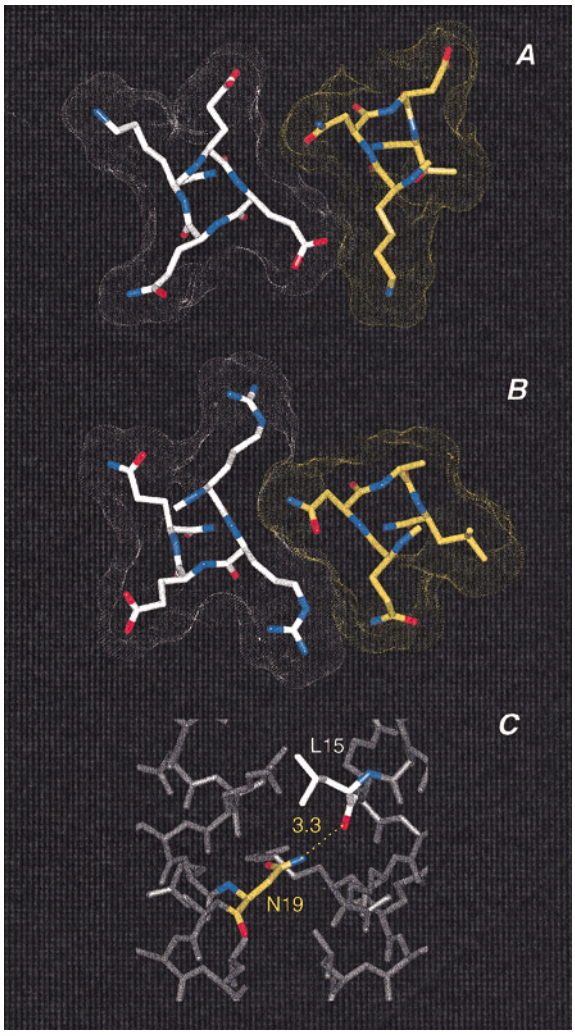

Figure 9. Cross-sectional views of c-Myc-Max r depicting the interfacial arrangement of Max Asn5*a* (A) and Max Asn19*a* (B) with the corresponding molecular surfaces. Note the parallel packing of the Asn side-chains as defined by the relative orientation of the C^{α}–C^{β} bonds and the peptide bond linking residues at positions *g* and *a* on the opposing helix (Harbury *et al*., 1993). C, Interhelical H-bond between the side-chain of Max Asn19*a* and the backbone carbonyl of c-Myc Leu15*d* as described in the text. Same color code as for Figure 6. Distances are given in Å. The Figure was generated using the program Insight II (Biosym, Palo Alto, CA).

LZ may allow the packing in the N-terminal region to be better defined.

As seen in Figure 9B, Max Asn19*a* packs between c-Myc Arg18*g* and Arg19*a*. Figure 9C indicates that the $N^{\delta 2}$ (and $H^{\delta 22}$) of Asn19*a* is engaged in a H-bond with the backbone carbonyl of c-Myc Leu15*d*. The donor acceptor distance is 2.2 Å and a N-H···O angle of 140° is observed. In opposition to the homodimeric case (O'Shea *et al.*, 1991; Junius *et al.*, 1995, 1996), no side-chain–side-chain H-bond across the interface is observed. Indeed, the H-bond donors of the guanidino group of c-Myc Arg19*a* are too distant in space from the $O^{\delta 1}$ of Max Asn19*a*. Solution NMR studies on the GCN4 (Oas *et al.*, 1990) and c-Jun homodimeric LZs (Junius *et al.*, 1993, 1995) have shown that only one set of resonances can be observed, leading to the hypothesis that the asparagine side-chains are flipping (around $\chi 2$) between two distinct, symmetry-related H-bonded conformations in the fast chemical exchange regime at room temperature (Junius *et al.*, 1995). This flip-flop has also been proposed to provide some conformational, entropic compensation for the unfavorable loss of solvation enthalpy of burying the polar asparagine side-chains at the interface of the dimer (Mackay *et al.*, 1996). No flip-flop of the side-chain of Max Asn19*a* is observed as evidenced from the extensive number of NOEs and the excellent definition of the side-chain. In addition, unlike the c-Jun homodimer case (Junius *et al.*, 1995), there was no attenuation of the $H^{\delta 2}$ signals at lower temperature. This attenuation was interpreted in terms of the flip-flop changing from a fast exchange regime to a medium exchange regime (Junius *et al.*, 1995; King, 1996). The fact that the $O^{\delta 1}$ of Max Asn19*a* is not accepting a H-bond and that a flip-flop is not observed suggests that a larger loss of solvation free energy upon burial is expected in the c-Myc-Max heterodimeric LZ compared to the GCN4 or c-Jun homodimers. Finally, the $\chi 1$ ($-70(\pm 12)°$) and $\chi 2$ ($-2(\pm 20)°$) values for the side-chain of Max Asn19*a* are very similar to those observed for the asparagine side-chain ($\chi 1 = -65°$ and $\chi 2 = 0.5°$) in the helix B of the GCN4 crystal structure (O'Shea *et al.*, 1991).

Figure 10B presents the kinetics of ^1H to ^2H exchange of the Max Asn19*a* $H^{\delta 22}$ at pD^{read} 5.8 and 20°C. The resonance of Max Asn19*a* $H^{\delta 22}$ is well resolved in one-dimensional spectra in H_2O (Figure 10A). The two $H^{\delta 2}$s appear to have similar rates of exchange as indicated by the fact that their intensities are the same after 45 minutes (Figure 10A). The rate of ^1H to ^2H exchange (k_{ex}) of Max Asn19*a* $H^{\delta 22}$ was obtained from the fitting of the curve in Figure 10B to a single exponential decay and is found to be $0.021(\pm 0.05)$ min^{-1}. Using exchange rate constants listed in Table IV of Bai *et al.* (1993); see Materials and Methods), we calculated a corresponding intrinsic or random coil (k_{rc}) rate of exchange of 1.89 min^{-1} at pD 5.8 and 20°C. Therefore, the protection factor ($PF = k_{rc}/k_{ex}$) against amide exchange is observed to be 90. Assuming an EX2 mechanism (Kim & Woodward, 1993; Bai *et al.*, 1994), that implies the ^1H to ^2H exchange to be controlled by the global opening (or global unfolding) of the structure, an opening equilibrium constant ($K_{op} = k_{ex}/k_{rc}$) of 0.011 is obtained. Correspondingly, a ΔG_{op} ($-RT \cdot \ln K_{op}$) of $2.60(\pm 0.65)$ kcal·mol^{-1} can be calculated. If the $H^{\delta 22}$ of Max Asn19*a* is buried at the interface of the folded form of c-Myc-Max heterodimeric LZ, then the ΔG_{op} value should be in agreement with the ΔG^u at 20°C and similar pH.

Figure 10C illustrates the temperature-induced denaturation curve of the disulfide-linked c-Myc-Max heterodimeric LZ monitored by CD at pH 6 (pD^{read} of 5.8 corresponds to approximately pH 6.2: Glasoe & Long, 1960). Figure 10D displays the corresponding stability curve (as obtained by fitting the denaturation curve as described in Materials and Methods) and the ΔG_{op} value obtained from the amide exchange experiment at 20°C. From the fit of the temperature-induced denaturation, we calculate the ΔG_u value at 20°C to be $1.8(\pm 0.4)$ kcal·mol^{-1}, which is somewhat lower but close to the ΔG_{op} ($2.60(\pm 0.65)$kcal·mol^{-1}) considering the uncertainties of the two values. Max Asn19*a* may be involved in some residual structure (secondary) in the unfolded state at 20°C and the k_{rc} value, which is obtained for an asparagine side-chain in a dipeptide, could be overestimated. Indeed, if Max Asn19*a* $H^{\delta 22}$ in the unfolded state is less solvent accessible than in a dipeptide, its intrinsic exchange should correspondingly be slower, leading to an overestimated ΔG_{op} value. But, the overall agreement between the ΔG_u and the ΔG_{op} values at 20°C lends credence to the fact that the $H^{\delta 22}$ of Max Asn19*a* is indeed buried at the interface of the structure and that it exchanges predominantly in the unfolded form of the disulfide-linked c-Myc-Max heterodimeric LZ.

On the basis of the structural, amide exchange and thermodynamic results presented here, it is clear that the $N^{\delta 2}$ of the side-chain of the conserved asparagine side-chains at positions *a* can form a stable H-bond with the backbone carbonyl of the preceding position *d* on the opposing helix in heterodimeric LZs. This is the first time that such an interaction is shown to occur in a heterodimeric LZ.

Evidence for e-g *salt bridges*

It has been reported that many of the side-chains found at positions *e* and *g* of the heptad repeats of coiled-coil forming proteins are ionizable (Hodges *et al.*, 1972; Mclachlan & Stewart, 1975; Stone *et al.*, 1975; Cohen & Parry, 1990). It has also been proposed that the side-chains at positions *e* and *g* can form favorable electrostatic interhelical interactions and bring the helices parallel and in register with the classical *i* to $i' - 5$, *e*-*g*′ or *e*′-*g* patterns (Hodges *et al.*, 1972; Stone *et al.*, 1975; Talbot & Hodges, 1982; Hodges, 1992, 1996; Zhou *et al.*, 1994a,b), which are referred to as *e*-*g* salt bridges hereinafter.

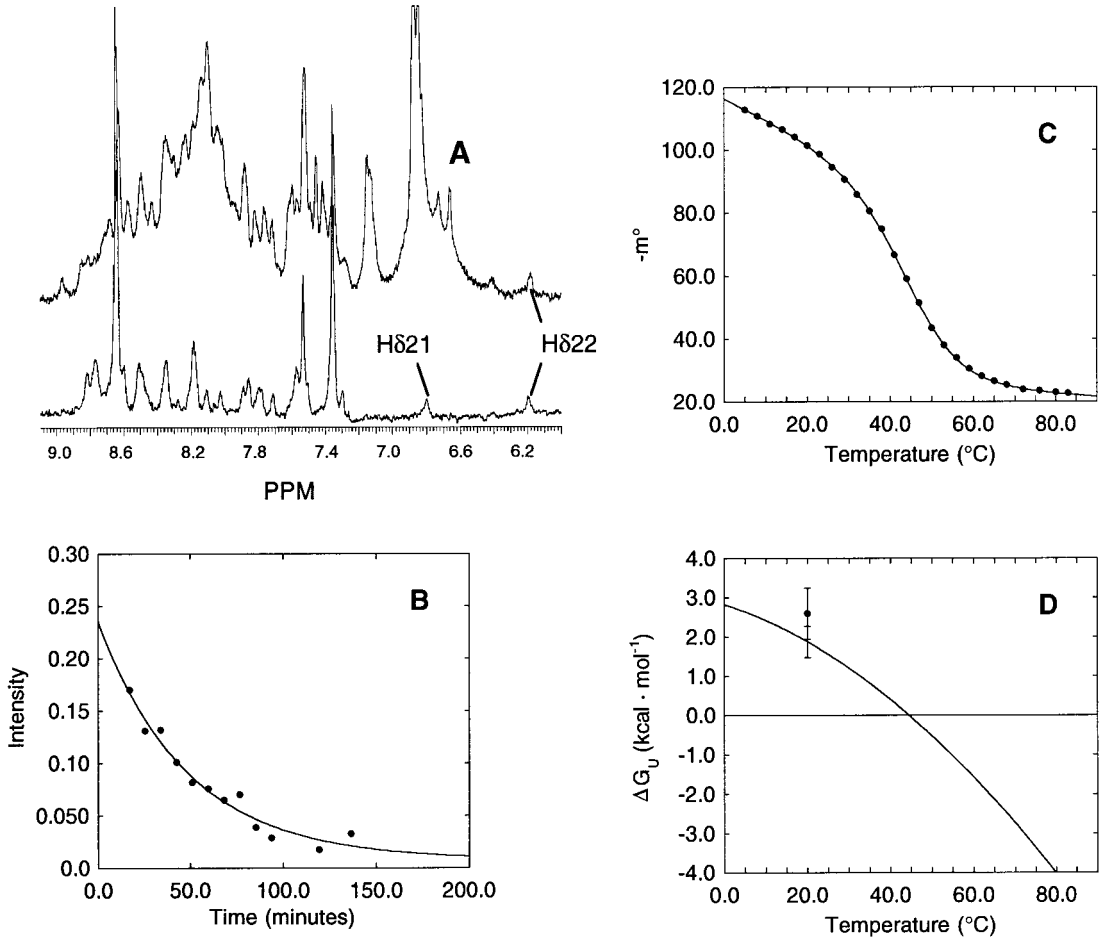

Figure 10. A, top, 500 MHz one-dimensional ^{1}H-NMR spectrum of the disulfide-linked c-Myc-Max heterodimeric coiled-coil acquired in 50 mM potassium phosphate, 50 mM KCl in 90% ^1H_2O, 10% ^2H_2O (pH 4.7); bottom, 500 MHz one-dimensional ^{1}H-NMR spectrum obtained 45 minutes after dissolution of the lyophilized sample in 100% ^2H_2O. B, ^{1}H to ^{2}H exchange kinetics of Max Asn19*a* $H^{\delta 22}$ at 293.15 K and pD^{read} 5.8. The exchange data were fitted to a single exponential decay (continuous line): the rate constant (k_{ex}) = 0.021(±0.05) min^{-1}. C, Temperature-induced denaturation of the disulfide-linked c-Myc-Max heterodimeric LZ recorded by monitoring the m° readings at 222 nm in 50 mM potassium phosphate, 50 mM KCl (pH 6.0). D, The corresponding stability curves obtained from the non-linear least-squares fitting as described in Materials and Methods. The fitted parameters obtained for the c-Myc-Max heterodimeric LZ (continuous line) are: $T^\circ = 44.5^\circ$C, $\Delta H^\circ_u = 31.4$ kcal·mol^{-1}, $\Delta C_{p,u} = 0.39$ kcal·mol^{-1}·K^{-1}, $m^\circ_N(0) = 117.0$, $dm^\circ_N(T)/dT = 0.62$, $m^\circ_U(0) = 29.15$, $dm^\circ_U(T)/dT = 0.11$. Also shown in D (filled circle) is the value of ΔG_{op} obtained from the rate of exchange of Max Asn19*a* $H^{\delta 22}$. See the text and Materials and Methods for further details.

Because positions *e* and *g* are contiguous to the canonical and mostly hydrophobic interfacial positions *a* and *d*, they form part of the hydrophobic core through the aliphatic part of their side-chains (O'Shea *et al.*, 1991). Correctly positioned *e-g* side-chains bearing like charges destabilize folded dimers (O'Shea *et al.*, 1989, 1992, 1993; Zhou *et al.*, 1994a; Kohn *et al.*, 1995). Such a destabilization of homodimers has been proposed to be the major driving force for the specific heterodimerization for the c-Fos and c-Jun LZs and synthetic LZs; whereas the formation of interhelical salt bridges in heterodimers is only thought to relieve the repulsions occurring in homodimers and not to provide electrostatic stabilization free energy (O'Shea *et al.*, 1992, 1993; Lumb & Kim, 1995b, 1996). Based on the fact that the pK_a values of two glutamate residues found to be involved in *e-g* salt bridges in the crystal structure of the GCN4 homodimeric LZ (O'Shea *et al.*, 1991) were not lower in the folded form than in the unfolded (p$K_{a,folded}$ < p$K_{a,unfolded}$) it was concluded that they were not providing any stability (or could even be destabilizing) through favorable electrostatic interactions (Lumb & Kim, 1995b, 1996). However, the absence of a pK_a shift does not automatically imply the absence of favorable electrostatic interactions (Yang & Honig, 1993; Lavigne *et al.*, 1996).

Three interhelical *e-g* salt bridges can be predicted to occur at the interface of the c-Myc-Max LZ: e.g. Max Asp11*g*–c-Myc Arg 16*e*, Max Lys16*e*–c-Myc Glu11*g*; and Max Glu23*e*–c-Myc Arg18*g* (Figure 1B).

In the final structure, the guanidino group of c-Myc Arg16*e* is found to be closer to the carboxylate groups of c-Myc Glu12*a* and c-Myc Asp13*b* than Max Asp11*g* as supported by the observation of medium range NOEs between the H^{δ}s and H^{ε} of c-Myc Arg16*e* and the H^{α} of c-Myc Asp13*b* (Figure 11A). The occurrence of two consecutive negatively charged side-chains on the c-Myc LZ should give rise to a high local electrostatic potential and therefore increase the probability of finding H-bond donors of the charged guanidino group of c-Myc Arg16*e* closer to c-Myc Glu12*a* and c-Myc Asp13*b* than Max Asp11 *g*. Moreover, H-bonds between guanadino group of c-Myc Arg16*e* and the carboxylate of c-Myc Glu12*a* could facilitate the burial of the latter, which has been shown to be involved in a buried salt bridge with Max His8*d* (Figure 11A).

Long range NOEs between the Max Lys16*e* H^{ε} and the methyl protons of c-Myc Leu15*d* indicates that the lysine side-chain is lining the interface and pointing in the direction of c-Myc Glu11*g* (Figure 11B). The distance between the carboxylate oxygens of c-Myc Glu11*g* and the Max Lys16*e* N^{ζ} is 5.8 Å indicative of a potential *e-g* electrostatic interaction. A lack of unambiguous NOEs for the side-chain protons of c-Myc Glu11*g* due to spectral overlap does not permit us to decide on the extent to which this salt bridge is populated. On the other hand and as illustrated on Figure 11B, interactions between the guanadino group of c-Myc Arg18*g* and the carboxylate of Max Glu23*e* are populated in solution as supported by many diagnostic NOEs involving the side-chain protons of Max Glu23*e* and c-Myc Arg18*g* and protons belonging to buried interfacial side-chains (Figure 11B).

Our results support the population of two *e-g* salt bridges at the interface of the disulfide-linked c-Myc-Max heterodimeric LZ at a pH of 4.8 and an ionic strength of 100 mM. To our knowledge, our results represent the first structural evidence that such interactions exist in solution.

Implications for the specific heterodimerization of the c-Myc and Max LZs

The mechanism for the specific heterodimerization of the LZ domains of transcription factors from the b-LZ family (e.g. the c-Fos-c-Jun system) has been characterized (O'Shea *et al.*, 1989, 1992). Destabilization through repulsion between interhelical like charges at *e* and *g* positions on the c-Fos LZ (O'Shea *et al.*, 1992) as well as the reduced stability of the c-Jun homodimeric LZ caused by the conserved asparagine side-chain at position *a* on the c-Jun LZ (Junius *et al.*, 1995, 1996) are two key factors of the specific heterodimerization and efficient reassortment in this system. The formation of interhelical *e-g′* salt bridges/H-bonds in the heterodimer is also thought to be important for molecular recognition although the magnitude of the contribution of these interhelical interactions to the stability of two-stranded α-helical coiled-coils is under debate (Lavigne *et al.*, 1996; Lumb & Kim, 1996). Upon inspection of the helical wheel diagrams of the Max and c-Myc homodimeric LZs, the hetero-

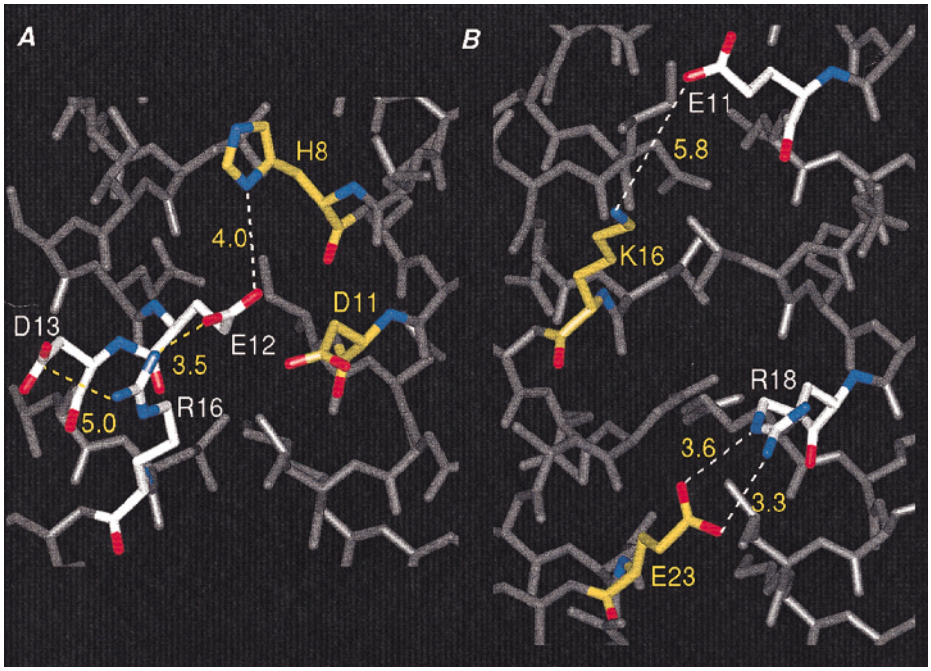

Figure 11. Interhelical and intrahelical interactions involving side-chains at positions *e* and *g*. A, Intrahelical interactions between c-Myc Arg16*e* and c-Myc Glu12*a* and c-Myc Asp13*b*. B, Interhelical salt bridges between Max Lys16*e* and c-Myc Glu11*g* and Max Glu23*e* and c-Myc Arg18*g*. Distances are given in Å. The Figure was generated using the program Insight II (Biosym, Palo Alto, CA).

dimerization specificity observed for the c-Myc and Max LZ does not seem to imply destabilization of homodimers through unfavourable *e-g* interhelical interactions. As a matter of fact, assuming the classical pattern (*e-g′* or *e′-g i* to *i′* − 5) no net repulsions can be predicted in both the Max and c-Myc homodimeric LZs (Lavigne *et al.*, 1995). On the other hand, the inability of c-Myc LZ to homodimerize at neutral pH has been argued to come mainly from the presence of two glutamate side-chains at positions *a* (Muhle-Goll *et al.*, 1994; Lavigne *et al.*, 1995). As discussed before, the occurrence of acidic side-chains (aspartic acid and glutamic acid) directly at the dimerization interface might prove to be a very effective mechanism of destabilization of homodimers (Lavigne *et al.*, 1995; Schneider *et al.*, 1997).

The reduced stability (compared to a generic parallel and two-stranded α-helical coiled-coil where all the positions *a* and *d* are occupied by hydrophobic residues) of the Max homodimeric LZ can be ascribed to the presence of the two asparagine residues at positions *a* and, intuitively, to the ionizable histidine at position *d*. As shown in this study and elsewhere (Muhle-Goll *et al.*, 1995), the presence of the two asparagine and the histidine residue does not prevent the homodimerization of the Max LZ (Figure 1). It is likely that the low stability of the Max homodimeric LZ is important in order to permit its reassortment with LZs belonging to its interacting partners.

In order for the c-Myc LZ (and hence the complete HLH-LZ motif) to heterodimerize, the burial or partial burial of two glutamate side-chains at positions *a* have to be compensated. The solution structure of the disulfide-linked c-Myc-Max LZ shows Max His8*d* as a key side-chain that allows heterodimerization and the partial burial of c-Myc Glu5*a* and c-Myc Glu12*a*. We have shown that the stability of the disulfide-linked c-Myc-Max LZ was greater at pH 5.0 than at pH 7.0 ($\Delta\Delta G_u = 0.95(\pm 0.40)$ kcal·mol^{-1}). This could be explained in part by the fact that upon decreasing the pH from 7.0 to 5.0, the population of protonated Max His8*d* ($pK_a = 7.2$ in the folded disulfide-linked c-Myc-Max LZ (Lavigne *et al.*, 1995) is increased from being roughly half at pH 7.0 to practically unity at pH 5.0, resulting in more favorable electrostatic interactions between Max His8*d* and c-Myc Glu5*a* and Glu12*a*. The ΔpK_a ($pK_{a,folded} - pK_{a,unfolded}$) of 0.42(±0.05) unit (corresponding to 0.57(±0.07) kcal·mol^{-1} at 25°C) observed for Max His8*d* supports this explanation (Lavigne *et al.*, 1995). It is clear that the pH dependence of the stability of the c-Myc-Max heterodimeric LZ is modulated in part or largely by the ionization state of Max His8*d*. At neutral pH where roughly half of Max His8*d* are neutral, charged H-bonds between it and c-Myc Glu5*a* and Glu12*a* can be formed and depending on the tautomeric form of the imidazole ring these charged H-bonds could facilitate the burial or partial burial of one or the other interfacial carboxylate on the c-Myc LZ.

Implications for regulation within the c-Myc network

In addition to the heterodimerization of the HLH-LZ domains, it is thought that the regulation of transcription as well as cell proliferation and differentiation by the proteins in the c-Myc network (Mad, Mxi1) relies on the temporal expression pattern of the *mad*, *mxi1* and *myc* genes (Littlewood & Evan, 1994; Henriksson & Lüscher, 1996; Hurlin *et al.*, 1997). For example, c-Myc, which is induced during cell proliferation, is down-regulated upon initiation of differentiation (Henriksson & Lüscher, 1996). An increase in the Mxi1 to c-Myc ratio and a switch from c-Myc-Max to Mxi1-Max heterodimer appears to be involved in the down-regulation of c-*myc* (Henriksson & Lüscher, 1996). Mad is also found to be induced at the onset of differentiation, indicating that both Mxi1-Max and Mad-Max heterodimers are important for differentiation (Henriksson & Lüscher, 1996). It appears that temporal shifts in relative amounts of Max heterodimers are at the center stage of the regulation of the c-Myc activities as well as cell growth and differentiation. In that regard, the low intrinsic stabilities for the Max homodimeric and the c-Myc-Max heterodimeric LZs are likely to be an advantage for the reassortment of the Max interacting proteins *in vivo*. Indeed, if the Max homodimeric and the c-Myc-Max heterodimeric LZs were highly stable, they would only allow for low populations of dissociated monomers and impede reassortment dictated by the level of expression of c-*myc*, *mad* and *mxi1* genes and transduction of cell growth and differentiation signals. Interestingly, the LZ domains of all the Max interacting proteins (Mad, Ayer *et al.*, 1993; Mad3 and Mad4, Hurlin *et al.*, 1995; Mxi1, Zervos *et al.*, 1993; Mnt, Hurlin *et al.*, 1997) have a conserved acidic residue (glutamic acid or aspartic acid) at the position analogous to c-Myc 5*a*. By preventing the homodimerization of the LZ domains due to repulsion and/or unfavorable desolvation effects, the occurrence of these acidic side-chains at position *a* in their LZ domains could explain why Max partner proteins are found not to dimerize or bind DNA. Again, this destabilization of homodimers is a prominent driving force for efficient heterodimerization. In addition, these conserved acidic residues are likely to be involved in the molecular recognition of Max through the formation of interfacial and favorable electrostatic/H-bond interactions with Max His8*d*, as demonstrated in this study for the c-Myc-Max heterodimeric LZ.

In conclusion, it was shown here that upon heterodimerization, the LZ domains of the c-Myc and Max proteins fold into a parallel and two-stranded α-helical coiled-coil. As discussed, the structure of the disulfide-linked c-Myc-Max heterodimeric LZ

reveals the existence of a specific interaction at the interface of the heterodimer between a histidine on the Max LZ and two glutamate residues on the c-Myc LZ that is proposed to play a crucial role for the molecular recognition of the two LZs. A similar interaction can be predicted to occur at the interface of all Max heterodimers as all Max b-HLH-LZ interacting partners known to date have a conserved acidic side-chain at the equivalent position to one of the glutamate residues on the c-Myc LZ. We suggest that the LZ domains of this sub-family of b-HLH-LZ proteins play a pivotal role in the heterodimerization and hence the cellular activities.

Materials and Methods

Peptide synthesis

Solid phase peptide synthesis of the c-Myc and the Max LZs, characterization by mass spectrometry, purification by reversed-phase HPLC and the formation of the disulfide-linked c-Myc and Max homodimeric LZs and the c-Myc-Max heterodimeric LZ have been described elsewhere (Lavigne *et al.*, 1995).

Temperature-induced denaturation monitored by circular dichroism

The temperature-induced denaturation curves monitored by CD have been acquired as described elsewhere (Lavigne *et al.*, 1995). The temperature dependence of mean residue ellipticity (Θ) or m° values at 222 nm have been fitted using an in-house non-linear least-squares fitting program assuming a two-state unfolding reaction as given below:

$$\Theta(T) = (1 - P_u(T)) \cdot \Theta_N(T) + P_u(T) \cdot \Theta_U(T)$$

where $\Theta_N(T)$ and $\Theta_U(T)$ and are the temperature dependence of the mean residue ellipticity of the macroscopic folded and unfolded states, respectively. They were both assumed to be linear, i.e. $\Theta_N(T) = \Theta_N(0) - d\Theta_N(T)/dT \cdot T$ and $\Theta_U(T) = \Theta_U(0) - d\Theta_U(T)/dT \cdot T$, where $\Theta_N(0)$ and $\Theta_U(0)$ are the mean residue ellipticities at 0°C for the folded and unfolded states, respectively; correspondingly $d\Theta_N(T)/dT$ and $d\Theta_U(T)/dT$ are the constant slopes of $\Theta_N(T)$ and $\Theta_U(T)$.

$P_u(T)$, the population of the unfolded state, is given by:

$$P_u(T) = \frac{\exp(-\Delta G_u(T)/RT)}{1 + \exp(-\Delta G_u(T)/RT)}$$

where the temperature dependence of the free energy of unfolding ($\Delta G_u(T)$) is described by:

$$\Delta G_u(T) = \Delta H_u^o\left(1 - \frac{T}{T^o}\right) + \Delta C_{p,u}(T - T^o) - T \ln\left(\frac{T}{T^o}\right)$$

where T^o is the melting temperature, ΔH_u^o is the apparent enthalpy of unfolding at T^o and $\Delta C_{p,u}$ is the temperature-independent heat capacity of unfolding. Although the $\Delta C_{p,u}$ value has been shown to depend on temperature (Makhatadze & Privalov, 1995; Gómez *et al.*, 1995), it is proposed that for temperatures up to 85°C it is a good approximation to consider $\Delta C_{p,u}$ temperature-independent (Gómez *et al.*, 1995).

Of the seven parameters used for the fitting of the temperature-induced denaturations curves, $\Delta C_{p,u}$ bears by far the largest standard deviation. Depending on the curve, the standard deviation can amount to a relative error of 50%. We rather measured an experimental $\Delta C_{p,u}$ value by plotting the apparent ΔH_u^o against T° obtained at five different pH values (3.0, 4.0, 5.0, 6.0 and 7.0). Both ΔH_u^o and T° were obtained graphically as described by Shortle *et al.* (1988) from van't Hoff analysis of the temperature denaturation curves of the disulfide-linked c-Max-Max heterodimeric LZ measured at the different pH values. The slope the relationship between ΔH_u^o and T° has been shown to correspond to $\Delta C_{p,u}$ (Privalov, 1979). By fitting the data to a straight line we obtained a $\Delta C_{p,u}$ of 0.39(±0.08) (or ±20%) kcal·mol^{-1}·K^{-1} with a correlation coefficient of 0.97, an indication that the $\Delta C_{p,u}$ can be assumed to be pH-independent. Therefore, in the fitting of the temperature-induced denaturation, $\Delta C_{p,u}$ was fixed to 0.39 and an error of at least 20% was assumed on the $\Delta G_u(T)$ obtained.

NMR spectroscopy

Six to 10 mg of the disulfide-linked c-Myc-Max heterodimeric LZ were dissolved in 0.5 ml of potassium phosphate buffer (50 mM, 10% ^2H_2O/90% ^1H_2O and pH 4.7 or 100% ^2H_2O) containing 50 mM KCl and 1 mM DSS (2,2-dimethyl-2-silapentane-5-sulfonic acid), to yield solutions ranging from 0.75 to 1.25 mM.

^1H homonuclear two-dimensional data acquisition and assignment

All the ^1H two-dimensional NMR spectra were recorded on a Varian VXR 500 or a Varian Unity 600 at 25°C. Proton resonances were assigned from DQF-COSY (Rance *et al.*, 1983), TOCSY (mixing time = 50 ms; Davis & Bax, 1985) and NOESY (mixing times = 50, 150 and 250 ms; Jeener *et al.*, 1979) experiments. Sequential assignment of the proton resonances was performed as described by Wüthrich (1986).

The spectra were acquired with 1024 or 2048 t_2 complex data points and 128 or 256 t_1 increments in the phase-sensitive mode with quadrature detection using the method described by States *et al.* (1982). Water resonance was suppressed during the 1.5 second relaxation period used in the NOESY, DQF-COSY and TOCSY experiments and the mixing period of the NOESY experiments by irradiating continuously at its resonance frequency.

Amide exchange

The amide exchange experiments were carried out by acquiring (after dissolving a ^1H lyophilized sample in 100% ^2H_2O) an arrayed set of one-dimensional spectra with an average elapsed time of 8.53 minutes between each spectrum. The spectra were acquired on a Varian Unity 300, at 20°C and pD^{read} 5.8. The relative intensities (I) were obtained by integration of the Max Asn19*a* resonance and fitted to a single exponential decay: $I = I^\circ \cdot \exp(-k_{ex} \cdot t) + I^\infty$, where I° is the fitted initial relative intensity, I^∞ is a baseline accounting for residual water ($^1H_20$) and k_{ex} is the desired rate of exchange.

A value of 0.39 min^{-1} for k_{rc} at 5°C and pD^{read} of 5.8 for Max Asn19*a* $H^{\delta 22}$ was obtained from the rate constants given in Table IV of Bai *et al.* (1993). As suggested by Bai *et al.* (1993), an activation energy of 17 kcal·mol^{-1}

was used to convert the calculated value of k_{rc} to 20°C, giving a value of 1.89 min^{-1} for Asn19*a* $H^{\delta 22}$.

Structure calculations

The intensities of the NOE crosspeaks from 50 ms and 150 ms NOESY experiments were measured and classified as strong, medium, weak and very weak. The crosspeak intensities were converted to interproton distances ranging between 1.8 and 2.8 Å (strong), 1.8 and 3.3 Å (medium), 1.8 and 4.0 Å (weak) and 1.8 and 5.0 Å (very weak).

To determine the χ^1 angles, it was assumed that the amino acid side-chains adopt one of three energetically favorable staggered conformations with $\chi^1 = +60°$, 180° or −60°. The side-chains analyzed were only restricted to a staggered conformation if the measured H^{α}-H^{β} coupling constants in a high resolution DQF-COSY spectrum were completely consistent with the intraresidue NH-H^{β} and H^{α}-H^{β} NOEs obtained in a 50 ms NOESY dataset. In addition, previous NMR assignments of LZs (Oas *et al.*, 1990; Junius *et al.*, 1993) have revealed that the β protons of the conserved leucine side-chains at positions *d* are characteristically split by almost 1 ppm with $H^{\beta 1}$ and $H^{\beta 2}$ having chemical shifts close to 1.3 and 2.2 ppm, respectively. Similar chemical shifts were observed in the present study and the NOEs observed were all consistent with the stereospecific assignments made.

In accordance with the helical medium range and sequential NOEs observed, poor coherence transfer was observed on the TOCSY spectra indicative of small $^3J_{HNH\alpha}$ (Cavanagh *et al.*, 1990) and α-helical like coupling constant (<5 Hz). Therefore, a φ angle of −60(±30)° was included for residues where more than three typical α-helical-like medium range and sequential connectivities were unambiguously assigned. The α-helical like φ angles used were further supported by the H^{α} chemical shift index (Wishart *et al.*, 1992). Fifty α-helical (CO-N (*i*, *i* + 4) 2.4 to 3.3 Å) hydrogen bond restraints were also used.

Calculations were performed using the program X-PLOR 3.1 (Brünger, 1992) and the dynamic simulated annealing protocol (Nilges *et al.*, 1988). This consisted of a total of 30 ps of high temperature dynamics (1000 K) followed by 20 ps of slow cooling (annealing) to 300 K. At 300 K a final stage of 400 steps of Powell minimization was performed. A total of 480 NOE distance restraints and 65 dihedral angles were included. Geometric center averaging was used for ambiguous assignments, e.g. methylene protons or methyl groups and pseudo-atoms were employed (Wüthrich *et al.*, 1983) with the appropriate upper bound corrections on the experimental restraints.

Solvent accessible surface areas were calculated using the program ANAREA (Richmond, 1984) as implemented in the program VADAR (Wishart *et al.*, 1994).

Coordinates have been deposited with the Brookhaven Protein Data Bank under accession codes 1a93 for the minimized averaged structure and 2a93 for the ensemble of 40 calculated structures.

Acknowledgements

We thank Bob Luty for CD measurements; Paul Semchuk, Leonard Daniels and Iain Wilson for peptide synthesis, purification and mass spectrometry. We also thank Gerry McQuaid and Bruce Lix for the maintenance of the NMR spectrometers, and Leigh Willard and Robert Boiko for their computer expertise. Drs Leslie Kondejewski, Michael Houston and Frank Sönnichsen are acknowledged for their invaluable help at the early stage of this project. We also thank the MRC group in protein structure and function for the use of the Varian VXR 500 spectrometer. This work was supported by the Protein Engineering Network of Centres of Excellence of Canada. P.L. acknowledges the Medical Research Council of Canada for a postdoctoral fellowship.

References

Amati, B., Dalton, S., Brooks, M. W., Littlewood, T. D., Evan, G. I. & Land, H. (1992). Transcriptional activation by the human c-Myc oncoprotein in yeast requires interaction with Max. *Nature,* **359**, 423–426.

Amati, B., Brooks, M. W., Levy, N., Littlewood, T. D., Evan, G. I. & Land, H. (1993). Oncogenic activity of the c-Myc protein requires dimerization with Max. *Cell,* **72**, 233–245.

Atkins, P. W. (1982). *Physical Chemistry*, W. H. Freeman and Company, San Francisco.

Ayer, D. E., Kretzner, L. & Eisenman, R. N. (1993). Mad: a heterodimeric partner for Max that antagonizes Myc transcriptional activity. *Cell,* **72**, 211–222.

Bai, Y., Milne, J. S., Leland, M. & Englander, S. W. (1993). Primary structure effects on peptide group hydrogen exchange. *Proteins: Struct. Funct. Genet.* **17**, 75–86.

Bai, Y., Milne, J. S., Leland, M. & Englander, S. W. (1994). Protein stability parameters measured by hydrogen exchange. *Proteins: Struct. Funct. Genet.* **20**, 4–14.

Battey, J., Moulding, C., Taub, R., Murphy, W., Stewart, T., Potter, H., Lenoir, G. & Leder, P. (1983). The human *c-myc* oncogene: structural consequences of translocation into the IgH locus in Burkitt lymphoma. *Cell,* **34**, 779–787.

Blackwood, E. M. & Eisenman, R. N. (1991). Max: a helix-loop-helix zipper protein that forms a sequence-specific DNA binding complex with Myc. *Science,* **251**, 1211–1217.

Blake, D. J., Tinsley, J. M., Davies, K. E., Knight, A. E., Winder, S. J. & Kendrick-Jones, J. (1995). Coiled-coil regions in the carboxy-terminal domains of dystrophin and related proteins: potentials for protein-protein interactions. *Trends Biochem. Sci.* **20**, 133–135.

Brünger, A. T. (1992). *X-PLOR Manual Version 3.1. A System for X-ray Crystallography and NMR*, Yale University Press, New Haven, CT.

Carson, M. (1987). Ribbon models of macromolecules. *J. Mol. Graph.* **5**, 103–106.

Cavanagh, J., Chazin, W. J. & Rance, M. (1990). The time dependence of coherence transfer in homonuclear isotropic mixing experiments. *J. Magn. Reson.* **87**, 110–131.

Chen, Y.-H., Yang, J. T. & Chau, K. H. (1974). Determination of the helix and β form of proteins in aqueous solution by circular dichroism. *Biochemistry,* **13**, 3350–3359.

Cohen, C. & Parry, D. A. D. (1990). α-Helical coiled-coils and bundles: how to design an α-helical protein. *Proteins: Struct. Funct. Genet.* **7**, 1–15.

Crick, F. H. C. (1953). The packing of α-helices: simple coiled-coil. *Acta Crystallog.* **6**, 689–693.

Davis, D. G. & Bax, A. (1985). Assignment of complex ^{1}H NMR spectra via two-dimensional homonuclear Hartmann-Hahn spectroscopy. *J. Am. Chem. Soc.* **107**, 2821–2822.

Ferré-D'Amaré, A. R., Prendergast, G. C., Ziff, E. B. & Burley, S. K. (1993). Recognition by Max of its cognate DNA through a dimeric b/HLH/Z domain. *Nature,* **363**, 38–45.

Glasoe, P. F. & Long, F. A. (1960). Use of glass electrode to measure acidities in deuterium oxide. *J. Phys. Chem,* **64**, 188–193.

Glover, J. N. M. & Harrison, S. C. (1995). Crystal structure of the heterodimeric bzip transcription factor c-Fos-c-Jun bound to DNA. *Nature,* **373**, 257–261.

Gómez, J., Hilser, V. J., Xie, D. & Freire, E. (1995). The heat capacity of proteins. *Proteins: Struct. Funct. Genet.* **22**, 404–412.

Gonzalez, L., Jr, Woolfson, D. N. & Alber, T. (1996). Buried polar residues and structural specificity in the GCN4 leucine zipper. *Nature Struct. Biol.* **3**, 1011–1018.

Goodman, E. M. & Kim, P. S. (1991). Periodicity of amide proton exchange rates in a coiled-coil leucine zipper peptide. *Biochemistry,* **30**, 11615–11620.

Harbury, P. B., Zhang, T., Kim, P. S. & Alber, T. (1993). A switch between two-, three- and four-stranded coiled-coils in GCN4 leucine zipper mutants. *Science,* **252**, 1401–1408.

Henriksson, M. & Lüscher, B. (1996). Proteins of the Myc network: essential regulators of cell growth and differentiation. *Advan. Cancer Res.* **68**, 109–182.

Hodges, R. S. (1992). Unzipping the secrets of coiled-coils. *Curr. Biol.* **2**, 122–124.

Hodges, R. S. (1996). *De novo* design of α-helical proteins: basic research to medical applications. *Biochem. Cell Biol.* **74**, 133–154.

Hodges, R. S., Sodek, J., Smillie, L. B. & Jurazek, L. (1972). Tropomyosin: amino acid sequence and coiled-coil structure. *Cold Spring Harbor Symp. Quant. Biol.* **37**, 299–310.

Hu, J. C. & Sauer, R. T. (1992). The basic-region leucine-zipper family of DNA binding proteins. *Nucl. Acids Mol. Biol.* **6**, 82–101.

Hurlin, P. J., Quéva, C., Koskinen, P. J., Steingrímsson, E., Ayer, D. E., Copeland, N. G., Jenkins, N. A. & Eisenmann, R. N. (1995). Mad3 and Mad4: novel Max-interacting transcriptonal repressors that suppress *c-myc* dependent transformation and are expressed during neural and epidermal differentiation. *EMBO J.* **14**, 5646–5659.

Hurlin, P. J., Quéva, C. & Eisenmann, R. N. (1997). Mnt, a novel Max-interacting protein is coexpressed with Myc in proliferating cells and mediates repression at Myc binding sites. *Genes Dev.* **11**, 44–58.

Hurst, H. (1994). Transcription factor I: b-zip proteins. *Protein Profile,* **1**, 123–152.

Jeener, J., Meier, B. H., Bachmann, P. & Ernst, R. R. (1979). Investigation of exchange processes by two-dimensional NMR spectroscopy. *J. Chem. Phys.* **71**, 4546–4553.

Junius, F. K., Weiss, A. S. & King, G. F. (1993). The solution structure of the leucine zipper motif of the jun oncoprotein homodimer. *Eur. J. Biochem,* **214**, 415–424.

Junius, F. K., Mackay, J. P., Bubb, W. A., Jensen, S. A., Weiss, A. S. & King, G. F. (1995). Nuclear magnetic resonance characterization of the jun leucine zipper domain: unusual properties of coiled-coil interfacial polar residues. *Biochemistry,* **34**, 6164–6174.

Junius, F. K., O'Donoghue, S. I., Nilges, M., Weiss, A. S. & King, G. F. (1996). High resolution NMR structure of the leucine zipper domain of the c-Jun homodimer. *J. Biol. Chem.* **271**, 13663–13667.

Kenar, K. T., García-Moreno, B. & Freire, E. (1995). A calorimetric characterization of the salt dependence of the stability of the GCN4 leucine zipper. *Protein Sci.* **4**, 1934–1938.

Kim, K.-S. & Woodward, C. (1993). Protein internal flexibility and global stability: effect of urea on hydrogen exchange rates of bovine pancreatic trypsin inhibitor. *Biochemstry,* **32**, 9609–9613.

King, G. F. (1996). NMR spectroscopy and X-ray crystallography provide complementary information on the structure and dynamics of leucine zippers. *Biophys. J.* **71**, 1152–54.

Kohn, W. D., Kay, C. M. & Hodges, R. S. (1995). Protein destabilization by electrostatic repulsions in the two-stranded α-helical coiled-coil/leucine zipper. *Protein Sci.* **4**, 237–250.

Kretzner, L., Blackwood, E. M. & Eisenman, R. E. (1992). The Myc and Max proteins possess distinct transcriptional activities. *Nature,* **359**, 426–429.

Kuntz, I. D., Kosen, P. A. & Craig, E. C. (1991). Amide chemical shifts in many helices and proteins are periodic. *J. Am. Chem. Soc.* **113**, 1406–1408.

Laskowski, R. A., MacArthur, M. W., Hutchinson, E. G. & Thornton, J. M. (1993). PROCHECK: a program to check the stereochemical quality of protein structures. *J. Appl. Crystallog.* **26**, 283–291.

Lavigne, P., Kondelewski, L. H., Houston, M. E., Jr, Sönnichsen, F. D., Lix, B., Sykes, B. D., Hodges, R. S. & Kay, C. M. (1995). Preferential heterodimeric parallel coiled-coil formation by synthetic Max and c-Myc leucine zippers: a description of putative electrostatic interactions responsible for the specificity of heterodimerization. *J. Mol. Biol.* **254**, 505–520.

Lavigne, P., Sönnichsen, F. D., Kay, C. M. & Hodges, R. S. (1996). Interhelical salt bridges, coiled-coil stability and specificity of dimerization. *Science,* **271**, 1136–1138.

Lavigne, P., Crump, M. P., Gagné, S. M., Sykes, B. D., Hodges, R. S. & Kay, C. M. (1997). ^{1}H-NMR evidence for two buried Asn side-chains in the c-Myc-Max heterodimeric α-helical coiled-coil. In *Techniques in Protein Chemistry*, vol. 8, pp. 617–624, Academic Press, San Diego.

Littlewood, T. D. & Evan, G. I. (1994). Transcription factors 2: helix-loop-helix. *Protein Profile,* **1**, 639–741.

Lumb, K. J. & Kim, P. S. (1995a). A buried polar interaction imparts structural uniqueness in a design heterodimeric coiled-coil. *Biochemistry,* **34**, 8642–8648.

Lumb, K. J. & Kim, P. S. (1995b). Measurement of interhelical electrostatic interactions in the GCN4 leucine zipper. *Science,* **268**, 436–439.

Lumb, K. J. & Kim, P. S. (1996). Interhelical salt bridges, coiled-coil stability and specificity of dimerization. *Science,* **271**, 1136–1138.

Mackay, J. P., Shaw, G. L. & King, G. F. (1996). Backbone dynamics of the c-jun leucine zipper: ^{15}N NMR relaxation studies. *Biochemistry,* **35**, 4867–4877.

Makhatadze, G. I. & Privalov, P. (1995). Energetics of protein structure. *Advan. Protein Chem.* **47**, 307–425.

McLachlan, A. D. & Stewart, M. (1975). Tropomyosin coiled-coil interactions: evidence for an unstaggered structure. *J. Mol. Biol.* **98**, 293–304.

Muhle-Goll, C., Gibson, T., Schuck, P., Nalis, D., Nilges, M. & Pastore, A. (1994). The dimerization stability of the HLH-LZ transcription protein is modulated by the leucine zippers: a CD and NMR study of TFEB and c-Myc. *Biochemistry,* **33**, 11296–11306.

Muhle-Goll, C., Nilges, M. & Pastore, A. (1995). The leucine zippers of the HLH-LZ proteins Max and c-Myc preferentially form heterodimers. *Biochemistry,* **34**, 13554–13564.

Nilges, M., Clore, G. M. & Gronenborn, A. M. (1988). Determination of the three-dimensional structure of proteins from interproton distances data by hybrid distance geometry-dynamical simulated annealing calculations. *FEBS Letters,* **229**, 317–324.

Oas, T. G., McIntosh, L. P., O'Shea, E. K., Dahlquist, F. W. & Kim, P. S. (1990). Secondary structure of a leucine zipper determined by nuclear magnetic resonance spectroscopy. *Biochemistry,* **29**, 2891–2894.

O'Shea, E. K., Ruthkowski, R., Stafford, W. F. & Kim, P. S. (1989). Preferential heterodimer formation by isolated leucine zippers from Fos and Jun. *Science,* **241**, 646–648.

O'Shea, E. K., Klemm, J. D., Kim, P. S. & Alber, T. (1991). X-ray structure of the GCN4 leucine zipper, a two-stranded, parallel coiled-coil. *Science,* **254**, 539–544.

O'Shea, E. K., Ruthkowski, R. & Kim, P. S. (1992). Mechanism of specificity in the Fos-Jun oncoprotein heterodimer. *Cell,* **66**, 699–708.

O'Shea, E. K., Lumb, K. J. & Kim, P. S. (1993). Peptide 'Velcro': design of a heterodimeric coiled-coil. *Curr. Biol.* **3**, 658–667.

Pardi, A., Wagner, G. & Wüthrich, K. (1983). Protein conformation and proton nuclear-magnetic-resonance chemical shift. *Eur. J. Biochem.* **137**, 445–454.

Prendergast, G. C., Lawe, D. & Ziff, E. B. (1991). Association of Myn, the murine homolog of Max, with c-Myc stimulates methylation sensitive DNA binding and Ras cotransformation. *Cell,* **65**, 395–407.

Privalov, P. (1979). Stability of proteins, small globular proteins. *Advan. Protein Chem.* **33**, 167–241.

Rance, M., Sørensen, O. W., Bodenhausen, G., Wagner, G., Ernst, R. R. & Wüthrich, K. (1983). Improved spectral resolution in COSY ^{1}H spectra of proteins via double quantum filtering. *Biochem. Biophys. Res. Commun.* **117**, 479–485.

Richmond, T. J. (1984). Solvent accessible surface area and excluded volume in proteins. *J. Mol. Biol.* **82**, 63–89.

Schneider, J. P., Lear, J. D. & DeGrado, W. F. (1997). A designed buried salt bridge in a heterodimeric coiled-coil. *J. Am. Chem. Soc.* **119**, 5742–5743.

Shortle, D., Meeker, A. K. & Freire, E. (1988). Stability mutants of staphylococcal nuclease: large compensating enthalpy-entropy changes for the reversible denaturation reaction. *Biochemistry,* **27**, 4761–4768.

States, D. J., Haberkorn, R. A. & Ruben, D. J. (1982). A two-dimensional nuclear Overhauser experiment with pure absorption phase in four quandrants. *J. Magn. Res.* **48**, 292–296.

Stone, D., Sodek, J. & Smillie, L. B. (1975). Tropomyosin: correlation of amino acid sequence and structure. In *Proceeding of the IX Federation of European Biochemical Societies Meeting, Proteins of Contractile Systems* (Bir, E. N. A., ed.), vol. 31, pp. 125–136, North Holland Publishing Co., Amsterdam.

Talbot, J. A. & Hodges, R. S. (1982). Tropomyosin: a model protein for studying coiled-coils and α-helix stabilization. *Acc. Chem. Res.* **15**, 224–230.

Wendt, H., Berger, C., Baici, A., Thomas, R. M. & Bosshard, H. R. (1995). Kinetics of folding of leucine zipper domains. *Biochemistry,* **34**, 4097–4107.

Wishart, D. S., Sykes, B. D. & Richards, F. M. (1992). The chemical shift index: a fast and simple method for the assignment of protein secondary structure through NMR spectroscopy. *Biochemistry,* **31**, 1647–1651.

Wishart, D. S., Willard, L., Richards, F. M. & Sykes, B. D. (1994). *VADAR: a Comprehensive Program for Protein Structure Evaluation. Version 1.2,* University of Alberta, Edmonton, Canada, Alberta.

Wishart, D. S., Bigam, C. G., Holm, A., Hodges, R. S. & Sykes, B. D. (1995). ^{1}H, ^{13}C and ^{15}N random coil NMR chemical shifts of the common amino acids. I. Investigations of nearest-neighbor effects. *J. Biomol. NMR,* **5**, 67–81.

Wüthrich, K. (1986). *NMR of Proteins and Nucleic Acids*, John Wiley & Sons, New York.

Wüthrich, K., Billeter, M. & Braun, W. (1983). Pseudo-structures for the 20 common amino acids for use in studies of protein conformations by measurements of intramolecular proton-proton distance constraints with nuclear magnetic resonance. *J. Mol. Biol.* **169**, 949–961.

Yang, A.-S. & Honig, B. (1993). On the pH dependence of protein stability. *J. Mol. Biol.* **231**, 459–474.

Zervos, A. S., Gyuris, J. & Brent, R. (1993). Mxi1, a protein that specifically interacts with Max to bind Myc-Max recognition sites. *Cell,* **72**, 223–232.

Zhou, N. E., Kay, C. M. & Hodges, R. S. (1994a). The role of interhelical ionic interactions in controlling protein folding and stability: *de novo* designed synthetic two-stranded α-helical coiled-coils. *J. Mol. Biol.* **237**, 500–512.

Zhou, N. E., Kay, C. M. & Hodges, R. S. (1994b). The net energetic contribution of interhelical electrostatic attractions to coiled-coil stability. *Protein Eng.* **7**, 1365–1372.

Edited by P. E. Wright

(Received 20 January 1998; received in revised form 21 April 1998; accepted 21 April 1998)